Helical Fasciculation of Bipolar and Horizontal Cell Neurites for Wiring With Photoreceptors in Macaque and Mouse Retinas

Yoshihiko Tsukamoto,[1,2] Kyoko Iseki,[3] and Naoko Omi[2]

[1]Department of Biology, Hyogo College of Medicine, Mukogawa, Nishinomiya, Hyogo, Japan
[2]Studio EM-Retina, Satonaka, Nishinomiya, Hyogo, Japan
[3]Laboratory for Retinal Regeneration, RIKEN Center for Developmental Biology, Minatojima Minamimachi, Chuo-ku, Kobe, Hyogo, Japan

Correspondence: Yoshihiko Tsukamoto, Department of Biology, Hyogo College of Medicine, Mukogawa, Nishinomiya, Hyogo 663-8501, Japan; ytsuka@hyo-med.ac.jp.

Received: July 20, 2020
Accepted: January 8, 2021
Published: January 28, 2021

Citation: Tsukamoto Y, Iseki K, Omi N. Helical fasciculation of bipolar and horizontal cell neurites for wiring with photoreceptors in macaque and mouse retinas. *Invest Ophthalmol Vis Sci.* 2021;62(1):31. https://doi.org/10.1167/iovs.62.1.31

Purpose. The three-dimensional configurations of rod and cone bipolar cell (BC) dendrites and horizontal cell (HC) processes outside rod and cone synaptic terminals have not been fully elucidated. We reveal how these neurites are mutually arranged to coordinate formation and maintenance of the postsynaptic complex of ribbon synapses in mouse and monkey retinas.

Methods. Serial section transmission electron microscopy was utilized to reconstruct BC and HC neurites in macaque monkey and mouse, including metabotropic glutamate receptor 6 (mGluR6)-knockout mice.

Results. Starting from sporadically distributed branching points, rod BC and HC neurites (B and H, respectively) took specific paths to rod spherules by gradually adjusting their mutual positions, which resulted in a closed alternating pattern of H–B–H–B neurites at the rod spherule aperture. This order corresponded to the array of elements constituting the postsynaptic complex of ribbon synapses. We identified novel helical coils of HC processes surrounding the rod BC dendrite in both mouse and macaque retinas, and these structures occurred more frequently in mGluR6-knockout than wild-type mouse retinas. Horizontal cell processes also formed hook-like protrusions that encircled cone BC and HC neurites below the cone pedicles in the macaque retina.

Conclusions. Bipolar and horizontal cell neurites take specific paths to adjust their mutual positions at the rod spherule aperture. Some HC processes are helically coiled around rod BC dendrites or form hook-like protrusions around cone BC dendrites and HC processes. Loss of mGluR6 signaling may be one factor promoting unbalanced neurite growth and compensatory neurite coiling.

Keywords: mGluR6, neural circuit, macaque monkey, rod bipolar cell, retinal horizontal cell, ribbon synapse, serial section electron microscopy

The retinal outer plexiform layer (OPL) contains multiple tiers of rod spherules and one tier of cone pedicles, which are sites of synaptic transmission from rods and cones to specific populations of bipolar cells (BCs) and horizontal cell (HCs). In mouse[1] and primate[2] retina, ON rod BC dendrites and HC axon terminal processes are selectively destined for rod spherules, whereas cone bipolar cell dendrites and HC dendritic processes are destined for cone pedicles.

The invagination pattern of BC and HC neurites in rod spherules varies among species. Missotten[3] reported one to five central (BC) elements in single spherules of the human retina, whereas Pan and Massey[4] reported only one HC process in single spherules of the rabbit retina. We have thus far observed one to four BC dendrites and one to three HC processes in single spherules of the macaque retina. However, in most rod spherules of the wild-type mouse retina (97%), two BC dendrites and two HC processes enter through the basal aperture to construct a postsynaptic complex, referred to as a tetrad, for ribbon synapses.[5] In the tetrad, each BC dendrite borders two HC processes and vice versa, thus forming a closed H–B–H–B pattern. By contrast, in metabotropic glutamate receptor 6 (mGluR6)-knockout mice, 29% of the spherules are invaginated with only one BC dendrite compared to about 3% of the spherules in wild-type mice.[6] Thus, both wild-type and mGluR6-knockout mice provide valuable model animals to examine how patterns of BC and HC neurites are coordinated as they project toward spherules and gather at the spherule apertures.

The precise configuration of BC dendrites and HC processes outside rod spherules and the mechanisms facilitating the specific targeting to ribbon synapses remain unclear. However, accumulating evidence suggests mutual interactions between the membranes of rod BC dendrites and HC processes. In normal mouse retinal development, rod BC dendrites extend from the apical processes of

Investigative Ophthalmology & Visual Science

neuroepithelial cells by postnatal day 5 and retain a neighbor–neighbor relationship with HC processes.[7] The HC processes first enter a spherule, followed by rod BC dendrites, leading to the formation of ribbon-associated postsynaptic complex by 2 weeks of age.[8–10] In null-mutant mice lacking key presynaptic molecules, such as Bassoon,[11] Cacn1f,[12–14] CaBP4,[15] and CNGA3/CNGB1,[16] the rod BC and HC neurites sprout outside the rod spherules and into the outer nuclear layer, frequently leading to co-fasciculation and the formation of ectopic synapses. Similar events also occur in mammals after retinal detachment.[17] These findings suggest the inherent capability of HC and rod BC neurites to execute flexible morphogenesis,[18] including co-fasciculation, through mutually associated elongation of the neurites.

In this study, serial section transmission electron microscopy was used to clarify the structural features of BC and HC neurites invaginating photoreceptor terminals in adult retina. First, we observed the configurations and projection paths of wild-type mouse rod BC dendrites and HC processes before invagination into the spherule. Second, we revealed a helically encircling structure in mGluR6-knockout mice and compared the features and frequency of these helical coils between mGluR6-knockout and wild-type mice. Third, we identified helical structures of HC processes encircling rod BC dendrites in a macaque retina. We also examined nearby areas below cone pedicles and identified hook-like structures of HC processes surrounding cone BC dendrites. Finally, we summarize various modes of fasciculation and their potential significance for synaptic wiring in the OPL.

Materials and Methods

Animals

Retinas were obtained from a 7-year-old female macaque monkey (*Macaca fuscata*) and eight mice, including four wild-types and four mGluR6-knockouts. From the macaque,[19] 817 radial sections were collected at 3 mm temporal to the foveal center. From mouse 1, a 9-week-old female wild-type (C57BL/6J),[20] 366 radial sections were obtained at the central retina. From mouse 2, a 30-week-old male mGluR6-knockout (*Grm6*$^{-/-}$, 129/SvJ × C57BL/6J),[21] 300 radial sections were obtained at the central retina. A series of 100 tangential sections of the central retina was obtained from each of mice 3 to 5, one 12-week-old and two 90-week-old wild-types (*Grm6*$^{+/+}$, 129/SvJ × C57BL/6J),[21] and from each of mice 6 to 8, one 12-week-old and two 90-week-old mGluR6-knockouts (*Grm6*$^{-/-}$, 129/SvJ × C57BL/6J).[21] The monkey was donated by the Psychophysical Research Group in the (former) Electrotechnical Laboratory of the Ministry of International Trade and Industry. All animal experimental procedures were approved by the Hyogo College of Medicine Committee on Animal Research and performed in accordance with both the Act on Welfare and Management of Animals issued by the government of Japan and the ARVO Statement for the Use of Animals in Ophthalmic and Vision Research.

Tissue Fixation and Sectioning

The monkey retina was fixed by dual intraocular and intravascular injection of aldehyde fixative, and the mouse retinas were fixed by a single intravascular injection of aldehyde fixative. Tissue blocks of the retina, with intact sclera and choroid, were isolated, post-fixed with an aqueous solution of 2% osmium tetroxide with or without 1% potassium ferricyanide, and stained en bloc with 3% uranyl acetate in 80% methanol. Blocks were embedded in araldite resin and cut into serial sections 90-nm thick using a Leica UCT Ultramicrotome (Leica Microsystems, Wetzlar, Germany). Sections were mounted on formvar-coated single-slot grids and stained with 3% uranyl acetate in 80% methanol and Reynold's lead citrate.

Electron Microscopy

Electron micrographs of the serial sections were acquired at both 400× and 3000× magnifications using a JEM-1220 electron microscope (Jeol Ltd., Tokyo, Japan) at the Joint-Use Research Facilities of the Hyogo College of Medicine. The lower-magnification images were enlarged 10-fold to 4000×, and the higher magnification images by fourfold to 12,000× for printed image analysis. We traced every neuronal process and marked the synapses and other features with color pens on transparent sheets. The digitized contour lines were processed using TRI/3D-SRF-R graphics software (Ratoc Systems International, Tokyo, Japan). Adobe Creative Suite 6 (Adobe Systems, San Jose, CA, USA) was used for graphic representation of digital images, and ImageJ (National Institutes of Health, Bethesda, MD, USA) was used for densitometry of the electron micrographs.

Statistical Analysis

Statistica 06J (Statsoft Japan, Tokyo, Japan) was used to perform a Student's *t*-test and Mann–Whitney *U* test. $^{*}P < 0.05$ was considered statistically significant.

Results

Fascicle Formation Outside the Rod Spherule

Cross-sections of neurites in the OPL of wild-type mouse retina revealed the typical spatial arrangement of two rod BC dendrites and two HC processes (Fig. 1A). The four processes are arranged linearly in the order H1–B1–H2–B2 from left to right, about 1 µm below the spherule aperture (270 in Fig. 1A; see also Figs. 1Bγ, 1C). Closer to the spherule base, these four neurites are arrayed in a tetragon such that B1 borders both H1 and H2 from the left and B2 borders both H1 and H2 from the right (278 in Fig. 1A; see also Figs. 1Bα, 1C). Along the path approaching the spherule base, H1 traverses from left to right across B1 for insertion between B1 and B2 (274 in Fig. 1A; see also Fig. 1Bβ). In other words, the H1 process projects toward the spherule as a partial right-handed helix that wraps around the B1 axis (Fig. 1C).

Figure 1D presents another example of a longitudinal section of neurites through the outside and inside of the spherule in wild-type mouse retina. The four processes are arranged in the linear order B2–H1–B1–H2 from left to right at approximately 1 µm from the spherule (Fig. 1Eα). Thus, at this level, H1 borders both B2 and B1, but H2 only borders B1. However, at the basal aperture of the rod spherule, these processes are again arranged in a tetragon, with H2 changing position from the right of B1 to the left of B1 so that B1 and B2 border both H1 and H2. That is, H2 transverses obliquely across B1 for insertion between B1 and B2 along the path; in other words, the H2 process in this case projects as a

Investigative Ophthalmology & Visual Science

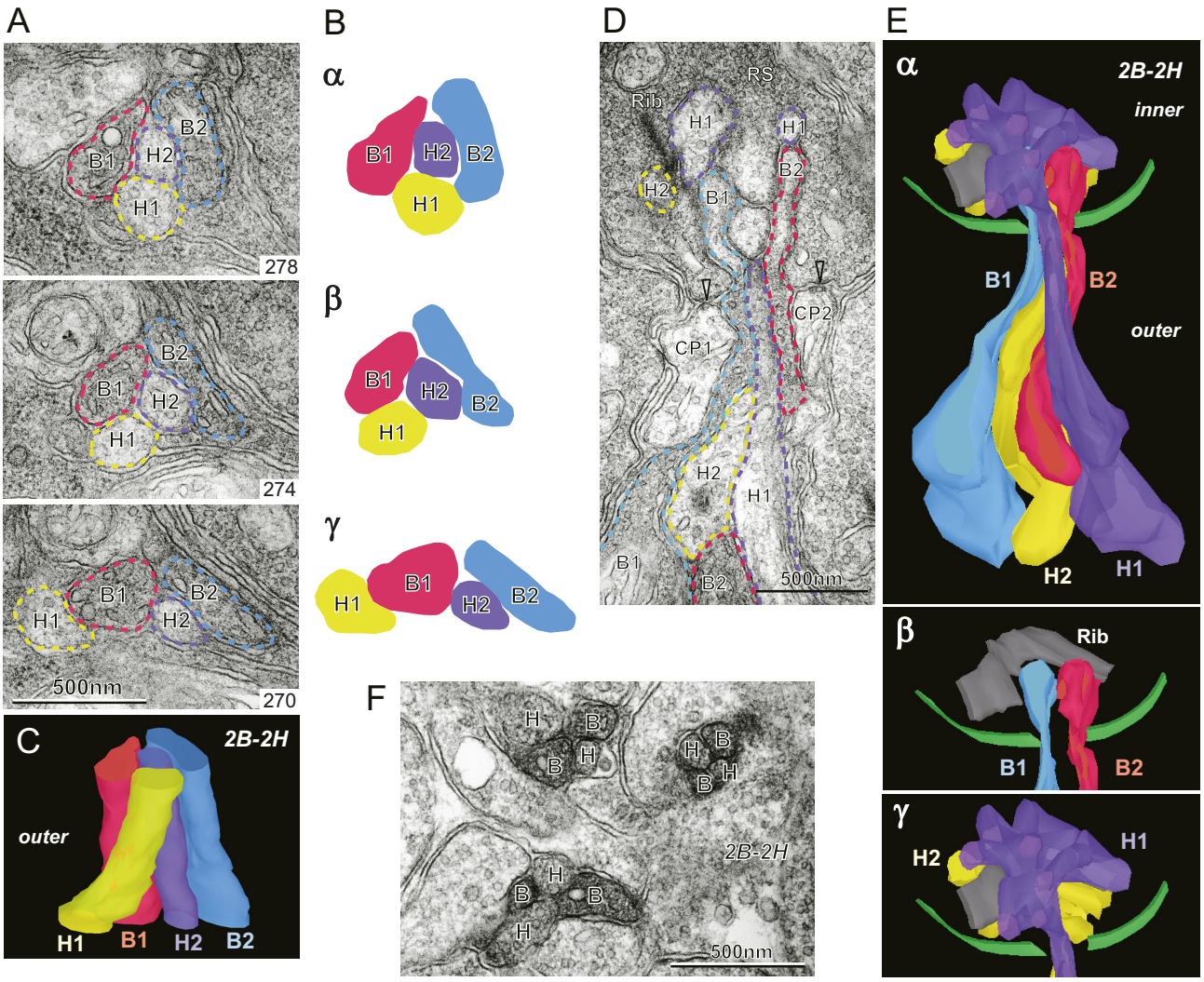

Figure 1. Morphological characteristics of 2B–2H-type neurite bundles below the rod spherule in wild-type mouse retina. (**A**) Electron micrographs of two rod BC dendrites and two HC processes in cross-section. All neurites eventually reach the entrance aperture of a rod spherule. (**B**) The transition from the H1–B1–H2–B2 linear array (*γ*) via the intermediate B1–H1–H2–B2 order (*β*) to the closed B1–H1–B2–H2 arrangement (*α*) as viewed from the top. (**C**) Illustration of **B** as viewed from the side. (**D**) Electron micrograph of two rod BC dendrites and two HC processes invaginating a rod spherule. (**E**) (*α*) The transition from the B2–H1–B1–H2 linear array below the aperture to the closed H2–B1–H1–B2 arrangement at the aperture; (*β*) illustration of B1 and B2 dendrites; (*γ*) illustration of H1 and H2 processes. (**F**) Electron micrograph of three H–B–H–B tetragonal arrangements at respective apertures.

partial left-handed helix around the B1 axis (Fig. 1E*α*). Inside the spherule, the ribbon-associated postsynaptic complex is comprised of B1 and B2 dendrites forming two parallel pillars and H1 and H2 processes forming flattened lobules. These neurites are regarded being arranged in a closed H–B–H–B array (Fig. 1E). Figure 1F shows three spherule apertures, at each of which a bundle of two rod BC dendrites and two HC processes forms a tetragonal pattern of H–B–H–B, where each rod BC dendrite borders both HC processes (H–B–H) and vice versa (B–H–B).

Helical Coils in the mGluR6-Knockout Mouse Retina

The helical coils of HC processes were first observed in mGluR6-knockout mouse retina, suggesting greater frequency in the absence of mGluR6 signaling. In some longitudinal sections of the rod BC dendrite (152 in Fig. 2A), transversely or obliquely cut tubular structures appeared to form a biserial array of slots flanking a slit (or a long narrow opening). In the next section (153 in Fig. 2A), these tubular segments resembled a ladder. Three-dimensional reconstruction of 15 images (Fig. 2B) showed that two HC processes encircled a common rod BC dendrite in a left-handed rotation, with each process making five turns. The helical coil shown in the figure was 2.3 µm long with 10 cycles and a mean pitch of 0.23 µm. These three neurites then projected together into a rod spherule. Although these HC helical structures were usually located outside spherules, they were also found occasionally within the spherules of mGluR6-knockout mouse retina (Figs. 2C–2E), and the shapes were more polymorphic inside than outside. One example exhibited a single turn encircling a rod BC dendritic tip (Fig. 2D), similar to the hook-like HC processes wrapping around rod BC dendrites found in rabbit rod spherules.[4] Such a

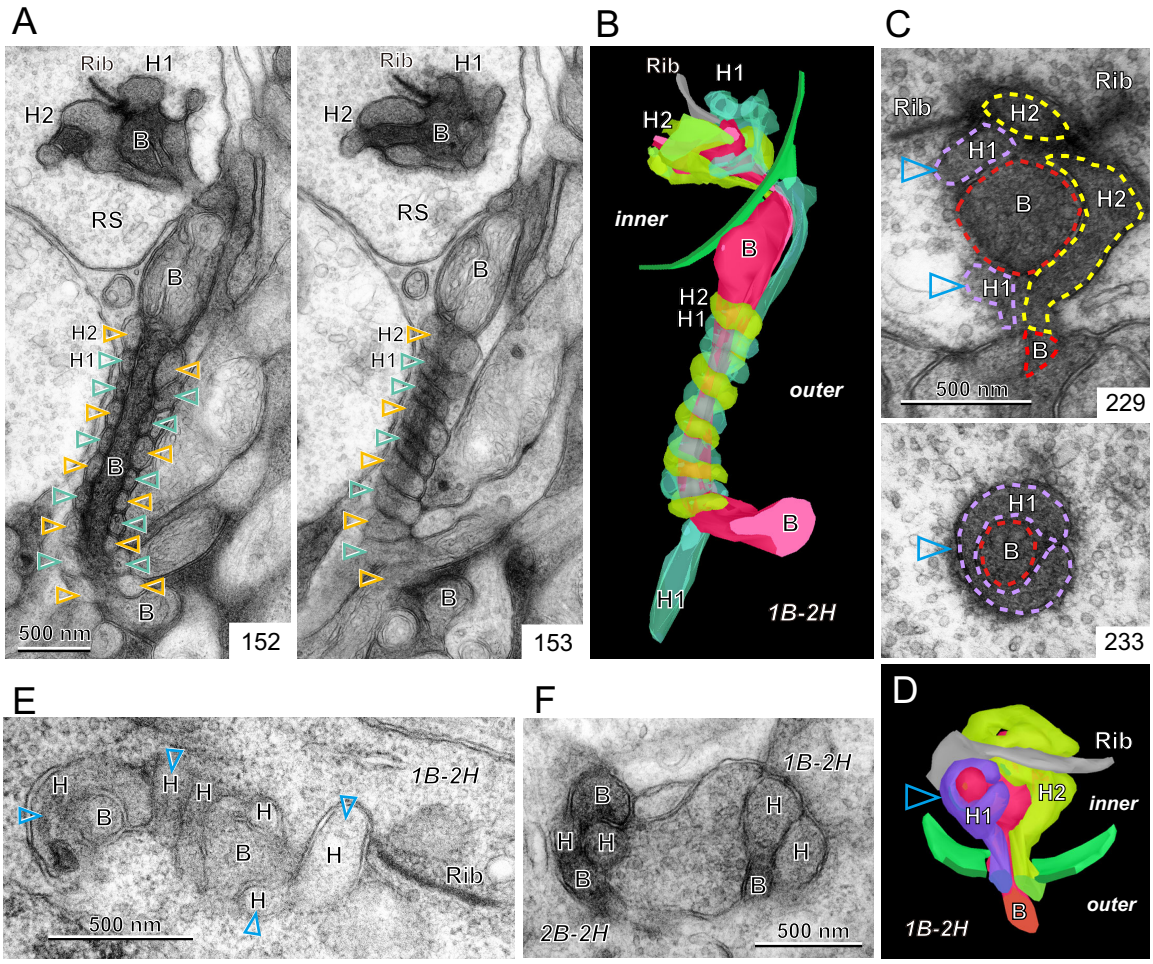

Figure 2. Configurations of HC processes surrounding rod BC dendrites in the mGluR6-knockout mouse retina. (**A**) Two adjacent HC processes surrounding a rod BC dendrite appear as biserial slots (*open arrowheads*) in slice 152 and with ladder-like profiles in slice 153. (**B**) A 3D model reconstructed from 15 serial micrographs of a 1B–2H type of fascicle. Note that two HC processes (H1, *blue–green*; H2, *yellow–green*) are helically coiled around a rod BC dendrite (B, *red*) in a left-handed rotation (2.3 µm long, 10 cycles). *Green*, spherule membrane; *gray*, ribbon synapse. (**C**) A 1B–2H type of fascicle invaginates a spherule. In slice 229, a longitudinal section through a rod BC dendrite is surrounded by the processes of two HCs. Slice 233 shows a cross-section of the rod BC dendritic tip encircled by an HC process. (**D**) A 3D model reconstructed from 14 serial micrographs of a ribbon synapse complex. (**E**) One rod BC and two HC neurites inside a spherule. Note the doughnut-like and ring-like shapes of the HC process. (**F**) Both H–B–H–B and H–B–H closed-loop arrangements are found at the apertures.

hook-like profile was not common inside the spherules of wild-type mice. The serial profiles of another example resembled ladders and slots surrounding a slit (Fig. 2E), similar to the helical structures observed outside spherules. This encirclement within spherules suggests the capability of the HC process to continue coiling around the rod BC dendrite.

The cross-sections of rod BC and HC neurite bundles at the spherule aperture showed 1B–2H as well as 2B–2H patterns (Fig. 2F), with the 1B–2H pattern being much more frequent in mGluR6-knockout mice than the wild-type mice, as observed in a previous study (29% of all bundles).[6]

Differences in Fasciculation Between Wild-Type and mGluR6-Knockout Mice

The doughnut-like profiles of HC process helical coils manifesting on cross-sections from mGluR6-knockout mice were also found in wild-type mice, although less frequently (Figs. 3A, 3B). At high magnification, electron-dense material was found in the cytoplasm of HCs facing the rod BC dendrite in both genotypes (Figs. 3C, 3D). At higher magnification, membranes of the HC process and the rod BC dendrite were observed in opposition across the interstitial cleft, and electron-dense fibrous material was observed on the intracellular side of the HC process membrane (Figs. 3E, 3F). Thus, specific conformations of cytoskeletal molecules may underlie the helical structure in both wild-type and mGluR6-knockout retinas.

To examine mGluR6-associated and age-related differences in these fasciculation patterns, we measured the number and the length of helical coils (defined as at least one complete circle around a rod BC dendrite) in an area (14 by 19 µm) of three wild-type and three mGluR6-knockout mouse retinas at 12 and 90 weeks of age (Figs. 3G, 3J, 3K). When a single rod BC dendrite had two separate

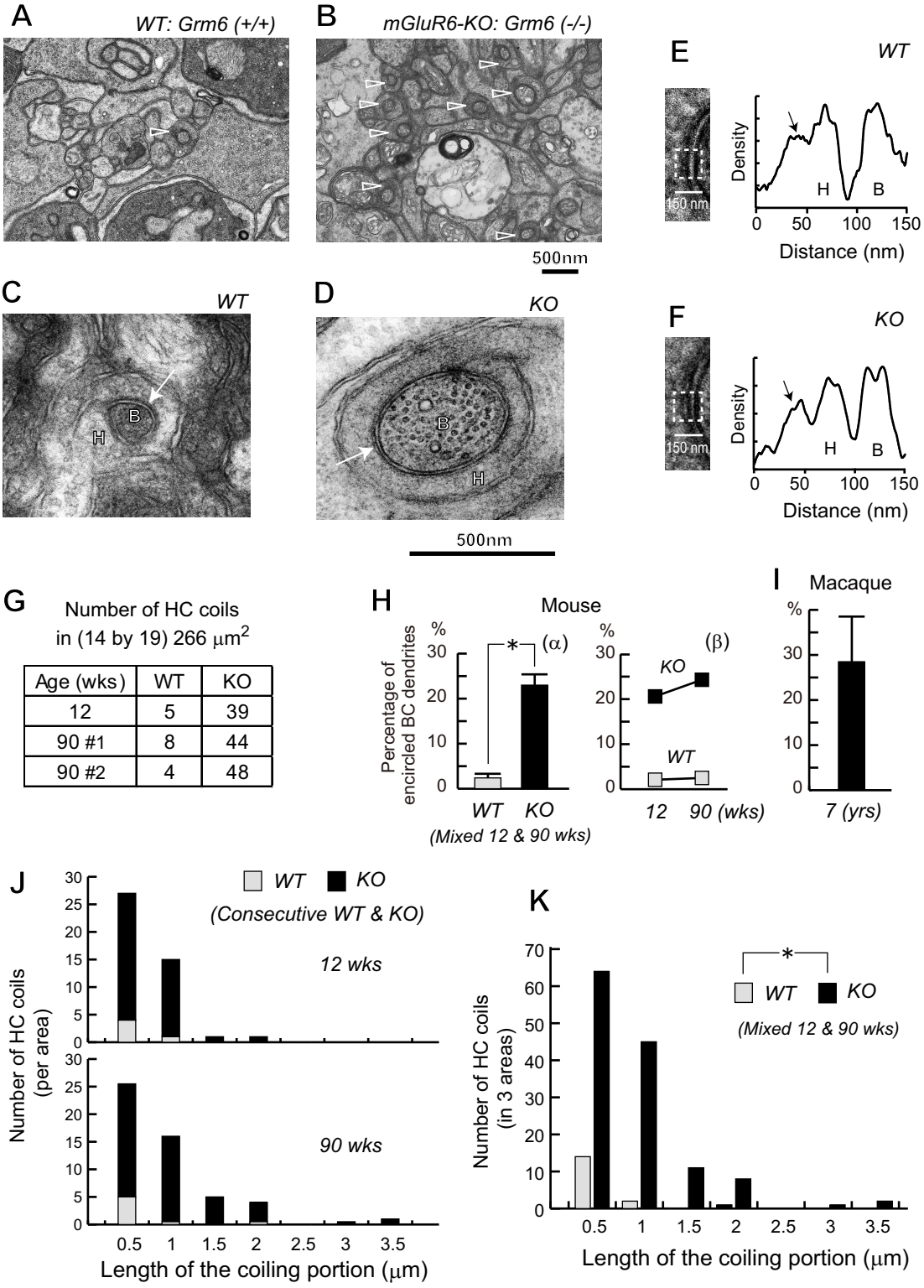

Age (wks)	WT	KO
12	5	39
90 #1	8	44
90 #2	4	48

Figure 3. Morphological comparison of coiled HC processes between wild-type (WT) and mGluR6-knockout (KO) mice. (**A**, **B**) Electron micrographs of HC processes in cross-section. The doughnut-shaped profiles are labeled by *arrowheads* at one site in the WT and eight sites in the KO retinal area. (**C**, **D**) An HC process is shown encircling a rod BC dendrite at higher magnification. (**E**, **F**) The H–B interfaces (*arrowheads* in **C** and **D**) were subjected to densitometry using ImageJ (the areas are indicated by dotted rectangles in **E** and **F**). A layer of dense material (*arrow*) was located on the intracellular side of the HC membrane. (**G**) Numbers of HC coils in the sampling area (14 × 19 μm) of WT and KO mouse retina at 12 weeks (one mouse) and 90 weeks (two mice). (**H**) Percentages of rod BC dendrites wrapped by HC coils. Comparisons between WT and KO mice (α) and between 12- and 90-week-old mice (β). (**I**) Percentages of rod BC dendrites wrapped by HC coils in the macaque retina ($n = 7$ rod BCs). (**J**) Histograms comparing coiled HC lengths between 12- and 90-week-old mice. (**K**) Histograms comparing coiled HC lengths between WT and KO mice. The length of a coil was measured by the number of cross-sections (0.09 μm thick) through which the coil passed.

Investigative Ophthalmology & Visual Science

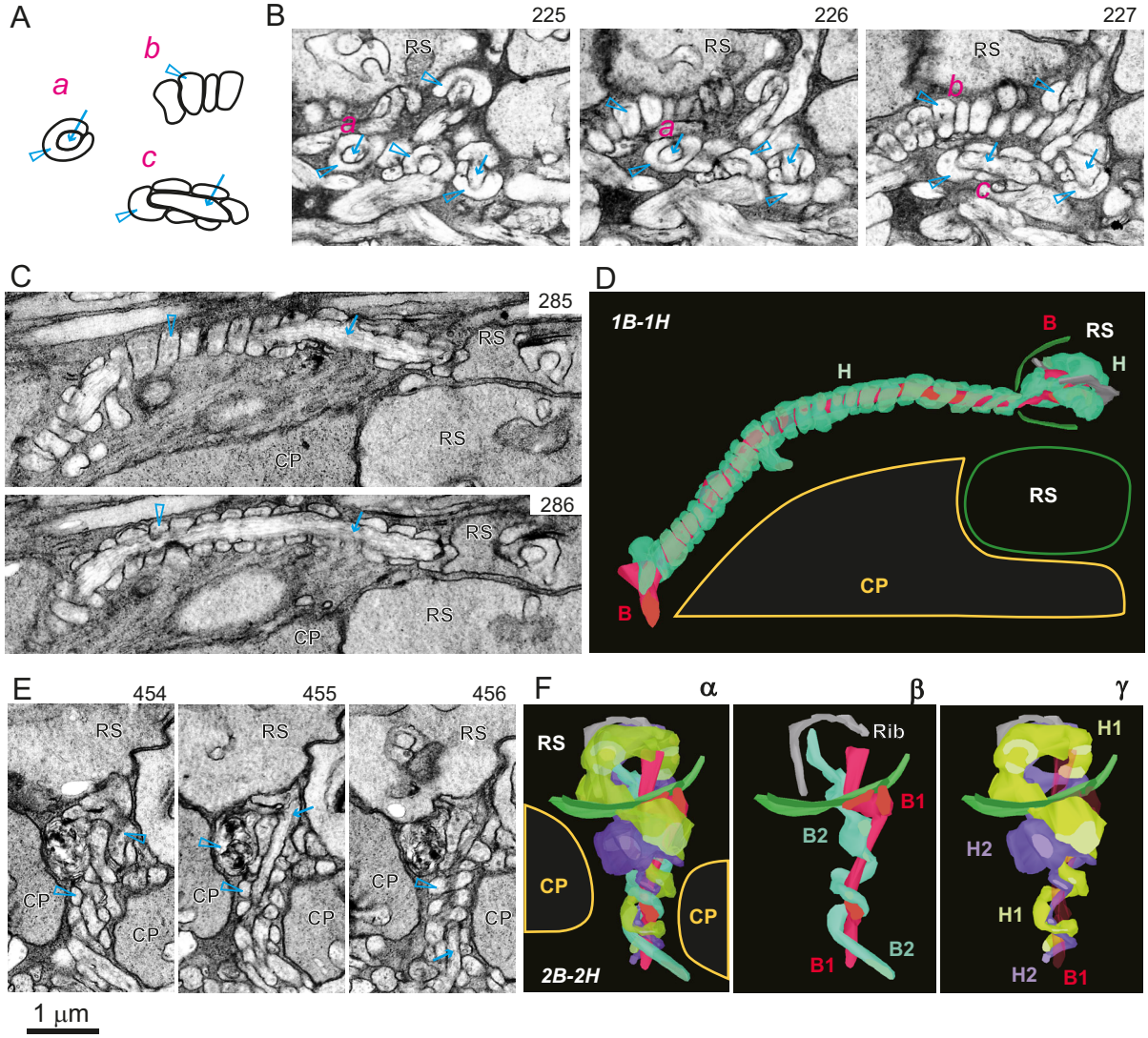

Figure 4. Electron micrographs of helical coils in the macaque retina. (**A**) The typical contours of helical coils: (**a**) doughnut-like; (**b**) ladder-like; (**c**) biserial slots flanking a slit. (**B**) A representative area displaying HC helical coils in the OPL. (**C**) The two consecutive images show characteristic shapes (285, ladder-like; 286, biserial slots) indicative of a helical HC process coiled around a rod BC dendrite. (**D**) A 3D model reconstructed from 26 serial micrographs of an HC helical coil (7 µm long, 20 cycles) surrounding a rod BC dendrite. The 1B–1H type of fascicle circumvents pedicles, invaginates into a spherule, and forms ribbon synapses at two active zones. (**E**) In a corridor among two pedicles and a spherule, rod BC and HC neurites show intricate shapes representing portions of three helical coils. (**F**) 3D models reconstructed from 31 serial micrographs of coiling and invaginating dendrites (2.5 µm long). (**α**) Complete profile of a 2B–2H type of fascicle with left-handed helical coils. (**β**) The dendrite of one rod BC (*blue*) coiled around the other rod BC (*red*). (**γ**) Two HC processes (*violet* and *yellow–green*) helically encircling one straight rod BC dendrite (*pale red*). Serial numbers of the slices are shown at the upper and lower right-hand sides. *Open arrowhead*, doughnut-like portion of the HC process (H); *arrow*, rod BC dendrite (B). RS, rod spherule; CP, cone pedicle.

segments with helical encirclement, we counted it as one case.

It was difficult to exactly count all the rod BC dendrites in our mouse samples, because rod BC dendrites, HC processes, and cone pedicle processes were piled up in the narrow interstitial space of five tiers of rod spherules. Therefore, we estimated the density of rod BC dendrites from the mean rod density and the mean divergence as described in Supplementary Table S1. Based on the numbers of rod BC dendrites in 266 µm^2, percentages of the rod BC dendrites encircled by HC coils were estimated to be 2.4% for wild-type and 23% for mGluR6-knockout mice (three mice for each genotype at mixed 12 and 90 weeks; unpaired, two-tailed Student's *t*-test, $^*P = 0.002$) (Fig. 3Hα). Thus, the HC coils around rod BC dendrites were approximately 10 times more frequent in mGluR6-knockout mice than wild-type mice (Fig. 3Hα). The HC coils occurred slightly more frequently at 90 weeks than at 12 weeks, but the *t*-test was not applicable due to the small sampling size (Fig. 3Hβ). The greatest length of the HC coiling portion was 2 µm in wild-type mice and 3.4 µm in mGluR6-knockout mice. The length distribution of HC coiling portions did not differ between ages ($n = 44$ per area at 12 weeks and $n = 52$ per area at 90 weeks; Mann–Whitney *U* test, $P = 0.32$) (Fig. 3J), but it did differ between

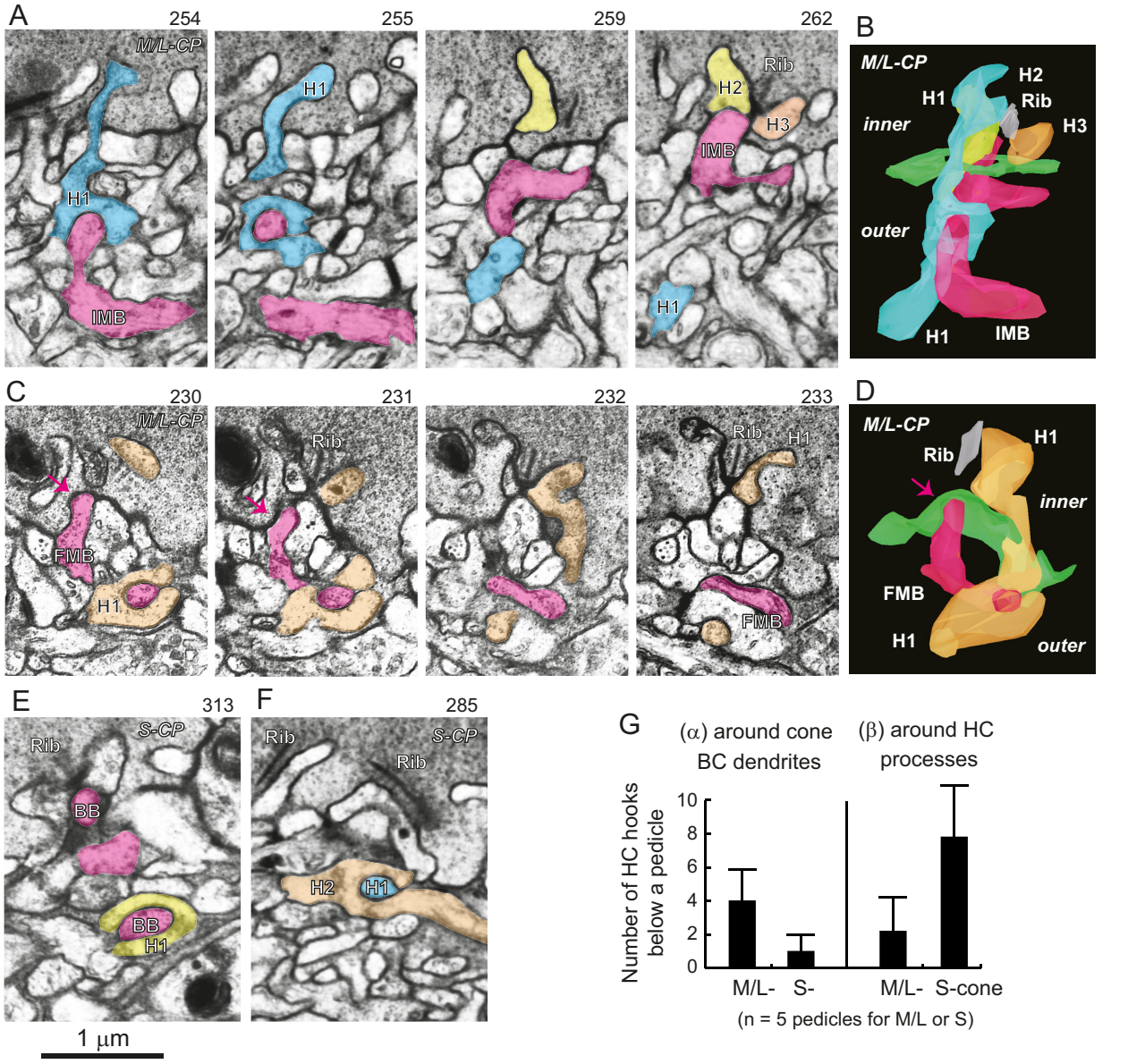

Figure 5. Encirclement of HC processes around the dendrites of cone BC and HC neurites below cone pedicles. (**A**) Consecutive micrographs of an HC process (H1 in *light blue*) encircling the dendrite of an IMB cell (*red*). (**B**) A 3D model reconstructed from 14 micrographs including **A**. The tip of the IMB dendrite forms the central element of a triad with two lateral HC processes (H2, *yellow*; H3, *orange*) under the ribbon (Rib). (**C**) Consecutive micrographs of an HC process (orange) encircling the dendrite of a FMB cell (*red*). (**D**) A 3D model reconstructed from 8 micrographs including **C**. The tip of the FMB dendrite contacts the pedicle base (*red arrow*). (**E**) Micrograph showing an HC process encircling the dendrite of a blue BC. (**F**) Micrograph showing the hook-like structure of an HC process surrounding another HC process. (**G**) The frequencies of HC hooks around cone BC dendrites (***α***) and HC processes (***β***) below a pedicle. Note that the area below S-cone pedicles (41 ± 6 μm^2, $n = 5$) is smaller than that below M/L-cone pedicles (57 ± 4 μm^2, $n = 5$) by a factor of 0.7.

genotypes ($n = 17$ in three areas of wild-type mice vs. $n = 131$ in three areas of mGluR6-knockout mice; Mann–Whitney U test, $^*P = 0.005$) (Fig. 3K).

Helical Coils in the Macaque Retina

There are two synaptic tiers in the OPL of the macaque retina. The innermost synaptic tier contains all cone pedicles and a small proportion of rod spherules, whereas the outer synaptic tiers contain the majority of rod spherules. Therefore, most rod BC dendrites and accompanying HC processes must pass through the innermost synaptic tier to reach target spherules in the outer synaptic tiers. Figure 4A shows three characteristic sectional profiles of helical coils in macaque retina: doughnut (a), ladder (b), and biserial slots flanking a slit (c). Figure 4B displays three consecutive slices (225–227) from an area of the OPL where all three characteristic profiles of helical encirclement are well developed.

A typical example of a ladder-like array is shown in slice 285 in Figure 4C and biserial slots flanking a slit in slice 286 in Figure 4C. The three-dimensional (3D) reconstruction from these two-dimensional cell contours revealed that the 1B–1H type of fascicle follows a relatively long path above the roof of a nearby pedicle before

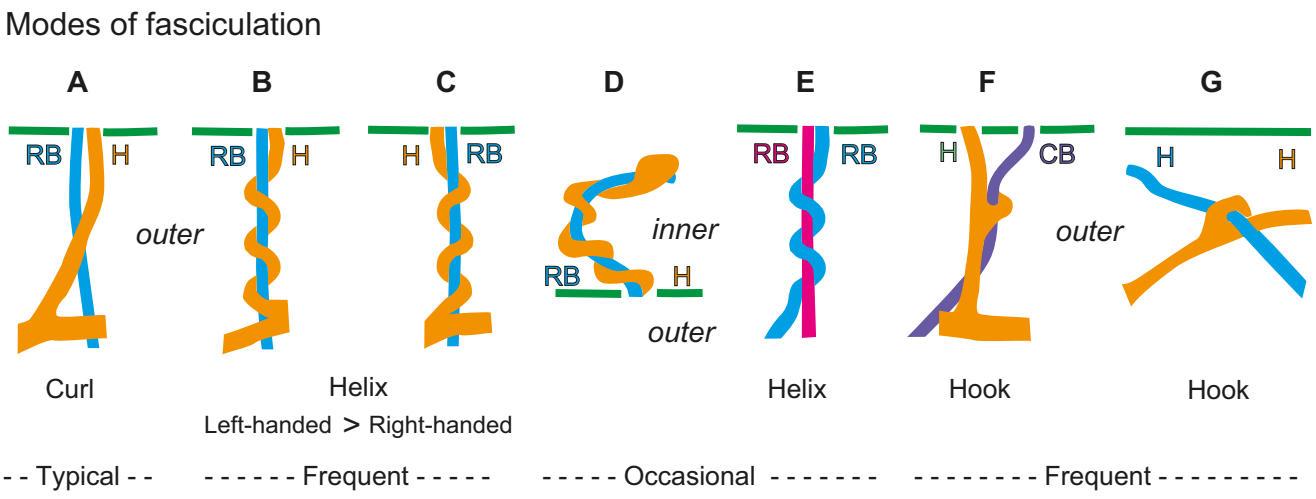

Figure 6. Various modes of fasciculation by bipolar and horizontal cell neurites as they project toward rod spherules (**A**–**E**) and cone pedicles (**F**, **G**). Mode **A** may occur for all neurites bundled together to adjust their mutual positions at the aperture. Modes **B** to **D** may occur in adult retina to allow elongated HC processes to fit within a fixed length of bundle. In a similar manner, mode **E** may adjust two different lengths of rod BC dendrite. Mode **F** may occur between HC dendrites and cone bipolar cell dendrites. Mode **G** may occur between two crossing HC neurites.

invaginating the target spherule (Figs. 4C, 4D). Another example area is shown in three consecutive slices (454–456) in Figure 4E. The 3D reconstruction shows that this 2B–2H type of fascicle projects between two pedicles to reach the target spherule (Fig. 4Fα). In this case, one rod BC dendrite (blue) encircles the other rod BC dendrite (red), with both dendrites entering the spherule and arriving close to the ribbon (gray) (Fig. 4Fβ). Two HC processes (yellow and violet) also encircle the rod BC dendrite (pale red), enter the spherule, and form terminal expansions to flank the rod BC dendrites (Fig. 4Fγ). These helical structures also have a left-handed rotation. The helical coils of HC processes encircling rod BC dendrites usually exhibited a left-handed rotation in both macaque and mouse retina; however, we observed several instances of right-handed helices in both species.

In the macaque retina, there were only two tiers of rod spherules compared to five tiers in the mouse retina; therefore, we were reliably able to identify almost all dendrites of each rod BC, as shown in Supplementary Table S2. The rod BC formed an average of 32 $\pm$ 2 invaginating dendrites ($n = 7$ cells), of which 9.1 $\pm$ 3.4 were encircled by HC helical coils. Thus, we estimated that 29% $\pm$ 10% of the dendrites were wrapped (Fig. 3I).

Hook-Like Protrusions Encircling Cone BC Dendrites

We did not observe any fascicles with helical coils below the cone pedicles in macaque retina but did detect hook-like encirclements by HC processes around cone BC dendrites and the other HC processes. We examined the areas below five pedicles for each group of medium- or long-wavelength-sensitive (M/L-) and short-wavelength-sensitive (S-) cones and found hook-like curved protrusions of HC processes encircling all (ON, OFF, midget, or diffuse) types of cone BC dendrites. The cases of an invaginating midget bipolar (IMB) cell and flat midget bipolar (FMB) cell are illustrated with 3D reconstructions in Figures 5A to 5D. The case of a blue bipolar cell is shown in Figure 5E. These HC processes and BC dendrites did not necessarily enter the same cone pedicle aperture; therefore, these hook-like protrusions did not form a tight bundle directed to a common target as seen in the rod–rod BC system. The HC protrusions also encircled the other nearby HC processes at their crossing points (Fig. 5F).

The HC hook-like protrusions were also quantitatively examined, as shown in Figures 5Gα–5Gβ. They were more numerous below M/L-cone pedicles (4 $\pm$ 1.9, $n = 5$) than S-cone pedicles (1 $\pm$ 1, $n = 5$); conversely, there were fewer HC hook-like protrusions around other HC processes below M/L-cone pedicles (2.2 $\pm$ 2.0, $n = 5$) than S-cone pedicles (7.8 $\pm$ 2.9, $n = 5$). It was difficult to determine the precise number of cone BC dendrites because they often branched intricately underneath the pedicles. Nonetheless, the numbers appeared to correlate slightly with the mean number of contacts with both M/L-cones (52 with ON-cone and 113 with OFF-cone BCs) and S-cones (42 with ON- and 53 OFF-cone BCs) reported in previous studies.[19,22] Thus, the fewer HC helical coils surrounding BC dendrites below S-cone pedicles is partly explained by the scarcity of cone BC dendrites synapsing with S-cones.

Discussion

Horizontal and bipolar cell neurites are capable of bundling in various configurations inside and outside the photoreceptor terminals. Inside the terminals, BC dendrite and HC processes construct postsynaptic complexes of ribbon synapses. Outside the terminals, the BC and HC neurites show several morphological modes of fasciculation (Fig. 6). For example, the linear configuration of four neurites (H–B–H–B) changes to the tetragonal configuration at the spherule aperture by pathway crossings (Fig. 1). More prominently, the helical coils of neurites and the encirclements by HC hook-like protrusions demonstrate flexible fasciculation. These configuration dynamics may be

Investigative Ophthalmology & Visual Science

essential for the precise targeting and maintenance of HC and BC neurites with specific rod and cone populations.

The targeting of HC and BC neurites to spherules depends on multiple guidance cues.[23] Mainly, netrin-G2 on the spherule and NGL-2 on the HC process have been shown to maintain the cell-autonomous rod–HC connections.[24,25] In addition, HC neurite pathfinding depends on repulsive interactions mediated by semaphorin 6A (Sema6A) and Plexin-A4[26] and elimination of excess HC neurites mediated by C1q.[27] Upon initial projection toward the rod spherule, the HC neurite is likely to arrive first at the aperture, with the rod BC dendrite arriving second.[8,10] The rod BC and HC projections adjust their mutual positions to develop smooth paths for synaptic wiring from the outside via the aperture into the active zones (Fig. 6A).

It has been suggested that the invagination of rod BC dendrites into rod spherules depends on two parallel transsynaptic bridges of the extracellular leucine-rich repeat fibronectin containing 1 (ELFN1)–mGluR6 complex[28,29] and the dystrophin–glycoprotein complex (DGC)–Pikachurin–G protein-coupled receptor 179 (GPR179) complex.[30–32] Here both *Elfn1*$^{-/-}$ and *Nob4* (a type of mGluR6-deficient mutant) mice exhibited defects in rod BC invagination.[28,33,34] It could then be hypothesized that mGluR6 deficiency may disrupt rod–rod BC transsynaptic adhesion. In the present study, however, rod–rod BC contact was preserved in mGluR6-knockout mice that were derived not from spontaneous mutations but from targeted disruption.[21] The same invagination event was observed in a total of 2100 rods in 13 mGluR6-knockout mice during our previous studies[6,35] and also by other researchers.[36] In addition, no physical interaction was detected between mGluR6 and Pikachurin.[31] In mGluR6-deficient mice (*Nob3*, *Grm6*$^{-/-}$),[37,38] GPR179 expression was significantly reduced but still retained at 30% to approximately 50% of the wild-type level. Therefore, we cannot ignore the possible role of the DGC–Pikachurin–GPR179 bridge in mGluR6-deficient mice.[32] The perplexing connections among molecules underlying selective synapse formation remain to be elucidated.

We speculate that neurites targeting the same spherule may elongate to different degrees. In this case, coiling the longer neurites around shorter neurites would be an effective way to maintain a common bundle length for precise spherule invagination. When HC processes grow more readily than rod BC dendrites, it necessitates the helical coiling of HC processes around rod BC dendrites (Figs. 6B–6D). Similarly, a longer rod BC dendrite may coil around a shorter dendrite within the same bundle (Fig. 6E).

This coiling appears to be sustained with age, as we found no significant difference in the length distribution of HC coiling portions between 12- and 90-week-old mice (Fig. 3). On the other hand, rod BCs tend to sprout ectopic dendrites into the outer nuclear layer in an age-dependent manner.[39] Our preliminary observations cannot exclude the possibility that HC processes elongate in an unbalanced manner with age, necessitating an increase in coiling, as our findings were obtained for only a few mice. Cone BC dendrites are greatly variable in direction and length depending on at least 11 different BC types. The reason for no HC helical coils below pedicles may be that BC and HC neurites have no common bundles with certain lengths for synaptic wiring. Nevertheless, HC processes have minute projections to hold nearby neurites, as we found HC hook-like protrusions below pedicles (Figs. 6F, 6G).

Acknowledgments

The authors thank T. Hamada for providing the monkey, M. Masu and C. Koike for comments, and T. Inoue and R. Fujimoto for technical assistance. We are grateful to our previous collaborators using mGluR6-KO mice, namely M. Azuma, M. Ishii, K. Morigiwa, M. Takao, S. Nakanishi, Y. Fukuda, and O. Mimura. YT designed the study and wrote the paper. YT, KI, and NO conducted the transmission electron microscopy experiments and data analysis.

Supported by a Japan Society for the Promotion of Science Grant-in-Aid for Scientific Research (22500317, YT).

Disclosure: **Y. Tsukamoto,** None; **K. Iseki,** None; **N. Omi,** None

References

1. Peichl L, Gonzalez-Soriano J. Morphological types of horizontal cell in rodent retinae: a comparison of rat, mouse, gerbil, and guinea pig. *Vis Neurosci*. 1994;11(3):501–517.
2. Kolb H. Organization of the outer plexiform layer of the primate retina: electron microscopy of Golgi-impregnated cells. *Philos Trans R Soc Lond B Biol Sci*. 1970;258(823):261–283.
3. Missotten L. *The Ultrastructure of the Retina*. Brussels: Arscia Uitgaven, N.V.; 1965.
4. Pan F, Massey SC. Rod and cone input to horizontal cells in the rabbit retina. *J Comp Neurol*. 2007;500(5):815–831.
5. Migdale K, Herr S, Klug K, et al. Two ribbon synaptic units in rod photoreceptors of macaque, human, and cat. *J Comp Neurol*. 2003;455(1):100–112.
6. Tsukamoto Y, Omi N. Effects of mGluR6-deficiency on photoreceptor ribbon synapse formation: comparison of electron microscopic analysis of serial sections with random sections. *Vis Neurosci*. 2014;31(1):39–46.
7. Morgan JL, Dhingra A, Vardi N, Wong RO. Axons and dendrites originate from neuroepithelial-like processes of retinal bipolar cells. *Nat Neurosci*. 2006;9(1):85–92.
8. Blanks JC, Adinolfi AM, Lolley RN. Synaptogenesis in the photoreceptor terminal of the mouse retina. *J Comp Neurol*. 1974;156(1):81–93.
9. Nemitz L, Dedek K, Janssen-Bienhold U. Rod bipolar cells require horizontal cells for invagination into the terminals of rod photoreceptors. *Front Cell Neurosci*. 2019;13:423.
10. Sherry DM, Wang MM, Bates J, Frishman LJ. Expression of vesicular glutamate transporter 1 in the mouse retina reveals temporal ordering in development of rod vs. cone and ON vs. OFF circuits. *J Comp Neurol*. 2003;465(4):480–498.
11. Specht D, Tom Dieck S, Ammermuller J, Regus-Leidig H, Gundelfinger ED, Brandstatter JH. Structural and functional remodeling in the retina of a mouse with a photoreceptor synaptopathy: plasticity in the rod and degeneration in the cone system. *Eur J Neurosci*. 2007;26(9):2506–2515.
12. Bayley PR, Morgans CW. Rod bipolar cells and horizontal cells form displaced synaptic contacts with rods in the outer nuclear layer of the nob2 retina. *J Comp Neurol*. 2007;500(2):286–298.
13. Chang B, Heckenlively JR, Bayley PR, et al. The *nob2* mouse, a null mutation in *Cacna1f*: anatomical and functional abnormalities in the outer retina and their consequences on ganglion cell visual responses. *Vis Neurosci*. 2006;23(1):11–24.
14. Mansergh F, Orton NC, Vessey JP, et al. Mutation of the calcium channel gene *Cacna1f* disrupts calcium signaling, synaptic transmission and cellular organization in mouse retina. *Hum Mol Genet*. 2005;14(20):3035–3046.
15. Haeseleer F, Imanishi Y, Maeda T, et al. Essential role of Ca2+-binding protein 4, a Cav1.4 channel regulator,

in photoreceptor synaptic function. *Nat Neurosci*. 2004; 7(10):1079–1087.

16. Michalakis S, Schaferhoff K, Spiwoks-Becker I, et al. Characterization of neurite outgrowth and ectopic synaptogenesis in response to photoreceptor dysfunction. *Cell Mol Life Sci*. 2013;70(10):1831–1847.
17. Fisher SK, Lewis GP, Linberg KA, Verardo MR. Cellular remodeling in mammalian retina: results from studies of experimental retinal detachment. *Prog Retin Eye Res*. 2005;24(3):395–431.
18. D'Orazi FD, Suzuki SC, Wong RO. Neuronal remodeling in retinal circuit assembly, disassembly, and reassembly. *Trends Neurosci*. 2014;37(10):594–603.
19. Tsukamoto Y, Omi N. OFF bipolar cells in macaque retina: type-specific connectivity in the outer and inner synaptic layers. *Front Neuroanat*. 2015;9:122.
20. Tsukamoto Y, Morigiwa K, Ueda M, Sterling P. Microcircuits for night vision in mouse retina. *J Neurosci*. 2001;21(21):8616–8623.
21. Masu M, Iwakabe H, Tagawa Y, et al. Specific deficit of the ON response in visual transmission by targeted disruption of the mGluR6 gene. *Cell*. 1995;80(5):757–765.
22. Tsukamoto Y, Omi N. ON bipolar cells in macaque retina: type-specific synaptic connectivity with special reference to OFF counterparts. *Front Neuroanat*. 2016;10:104.
23. Martemyanov KA, Sampath AP. The transduction cascade in retinal ON-bipolar cells: signal processing and disease. *Annu Rev Vis Sci*. 2017;3:25–51.
24. Soto F, Watkins KL, Johnson RE, Schottler F, Kerschensteiner D. NGL-2 regulates pathway-specific neurite growth and lamination, synapse formation, and signal transmission in the retina. *J Neurosci*. 2013;33(29):11949–11959.
25. Soto F, Zhao L, Kerschensteiner D. Synapse maintenance and restoration in the retina by NGL2. *Elife*. 2018;7: e30388.
26. Matsuoka RL, Jiang Z, Samuels IS, et al. Guidance-cue control of horizontal cell morphology, lamination, and synapse formation in the mammalian outer retina. *J Neurosci*. 2012;32(20):6859–6868.
27. Burger CA, Jiang D, Li F, Samuel MA. C1q regulates horizontal cell neurite confinement in the outer retina. *Front Neural Circuits*. 2020;14:583391.
28. Cao Y, Sarria I, Fehlhaber KE, et al. Mechanism for selective synaptic wiring of rod photoreceptors into the retinal circuitry and its role in vision. *Neuron*. 2015;87(6):1248–1260.
29. Dunn HA, Patil DN, Cao Y, Orlandi C, Martemyanov KA. Synaptic adhesion protein ELFN1 is a selective allosteric modulator of group III metabotropic glutamate receptors *in trans*. *Proc Natl Acad Sci USA*. 2018;115(19):5022–5027.
30. Omori Y, Araki F, Chaya T, et al. Presynaptic dystroglycan-pikachurin complex regulates the proper synaptic connection between retinal photoreceptor and bipolar cells. *J Neurosci*. 2012;32:6126–6137.
31. Orlandi C, Omori Y, Wang Y, et al. Transsynaptic binding of orphan receptor GPR179 to dystroglycan-Pikachurin complex is essential for the synaptic organization of photoreceptors. *Cell Rep*. 2018;25(1):130–145.e5.
32. Furukawa T, Ueno A, Omori Y. Molecular mechanisms underlying selective synapse formation of vertebrate retinal photoreceptor cells. *Cell Mol Life Sci*. 2020;77(7):1251–1266.
33. Cao Y, Masuho I, Okawa H, et al. Retina-specific GTPase accelerator RGS11/Gβ5S/R9AP is a constitutive heterotrimer selectively targeted to mGluR6 in ON-bipolar neurons. *J Neurosci*. 2009;29(29):9301–9313.
34. Pinto LH, Vitaterna MH, Shimomura K, et al. Generation, identification and functional characterization of the *nob4* mutation of *Grm6* in the mouse. *Vis Neurosci*. 2007;24(1):111–123.
35. Ishii M, Morigiwa K, Takao M, et al. Ectopic synaptic ribbons in dendrites of mouse retinal ON- and OFF-bipolar cells. *Cell Tissue Res*. 2009;338(3):355–375.
36. Kozuka T, Chaya T, Tamalu F, et al. The TRPM1 channel is required for development of the rod ON bipolar cell-AII amacrine cell pathway in the retinal circuit. *J Neurosci*. 2017;37(41):9889–9900.
37. Orlandi C, Cao Y, Martemyanov KA. Orphan receptor GPR179 forms macromolecular complexes with components of metabotropic signaling cascade in retina ON-bipolar neurons. *Invest Ophthalmol Vis Sci*. 2013;54(10):7153–7161.
38. Ray TA, Heath KM, Hasan N, et al. GPR179 is required for high sensitivity of the mGluR6 signaling cascade in depolarizing bipolar cells. *J Neurosci*. 2014;34(18):6334–6343.
39. Liets LC, Eliasieh K, van der List DA, Chalupa LM. Dendrites of rod bipolar cells sprout in normal aging retina. *Proc Natl Acad Sci USA*. 2006;103(32):12156–12160.

Investigative Ophthalmology & Visual Science